

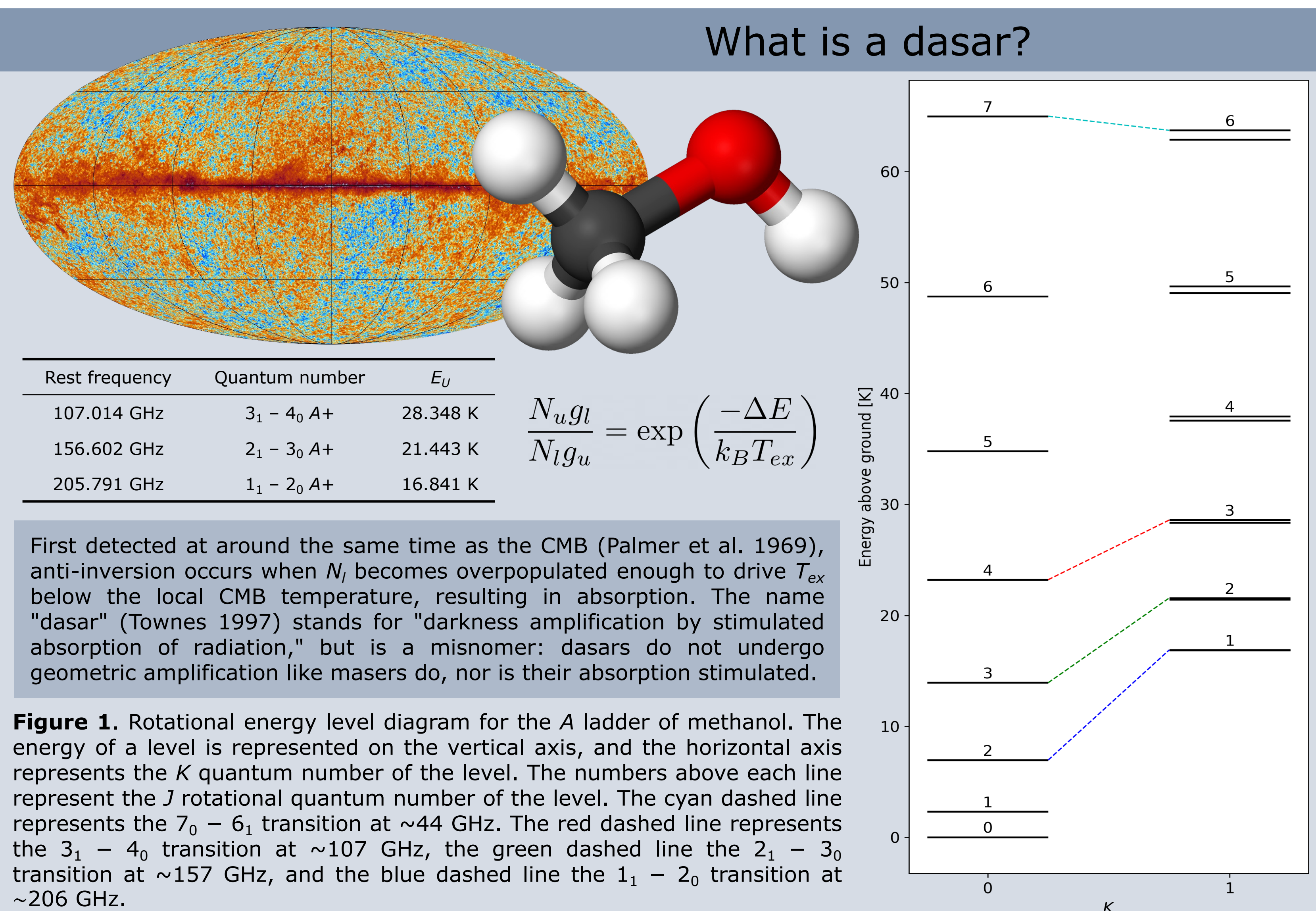
A methanol deep field survey of distant galaxies with ngVLA using dasars

Alyssa Bulatek (she/her)¹, Adam Ginsburg¹, Jeremy Darling², Christian Henkel^{3,4,5}, Karl M. Menten³

1. University of Florida, 2. Center for Astrophysics and Space Astronomy, CU Boulder, 3. Max-Planck-Institut für Radioastronomie, 4. King Abdulaziz University, 5. Xinjiang Astronomical Observatory

Motivation

Transitions between energy levels can become anti-inverted when a pumping mechanism drives a population of molecules into the lower state of a two-state system. This anti-inversion phenomenon, which has been called dasar absorption, makes the excitation temperature of the molecule so low that it can absorb cosmic microwave background (CMB) photons. Because dasars are absorption lines, their strength does not fall off with distance when the absorber is resolved, which makes them potentially powerful tools for measuring the physical conditions in distant galaxies. CH₃OH (methanol) has several transitions that are expected to dase at radio frequencies. We demonstrate with ALMA that the 107 GHz transition of methanol is a dasar in a Galactic target, specifically The Brick. We outline the possibilities of a deep field survey using the ngVLA to observe the methanol dasar transition at 107 GHz and potentially other transitions that may dase to study high-redshift starbursting galaxies.



First detected at around the same time as the CMB (Palmer et al. 1969), anti-inversion occurs when N becomes overpopulated enough to drive T_{ex} below the local CMB temperature, resulting in absorption. The name "dasar" (Townes 1997) stands for "darkness amplification by stimulated absorption of radiation," but is a misnomer: dasars do not undergo geometric amplification like masers do, nor is their absorption stimulated.

Figure 1. Rotational energy level diagram for the A ladder of methanol. The energy of a level is represented on the vertical axis, and the horizontal axis represents the K quantum number of the level. The numbers above each line represent the J rotational quantum number of the level. The cyan dashed line represents the $7_0 - 6_1$ transition at ~44 GHz. The red dashed line represents the $3_1 - 4_0$ transition at ~107 GHz, the green dashed line the $2_1 - 3_0$ transition at ~157 GHz, and the blue dashed line the $1_1 - 2_0$ transition at ~206 GHz.

Detection of absorption against the CMB in G0.253+0.016

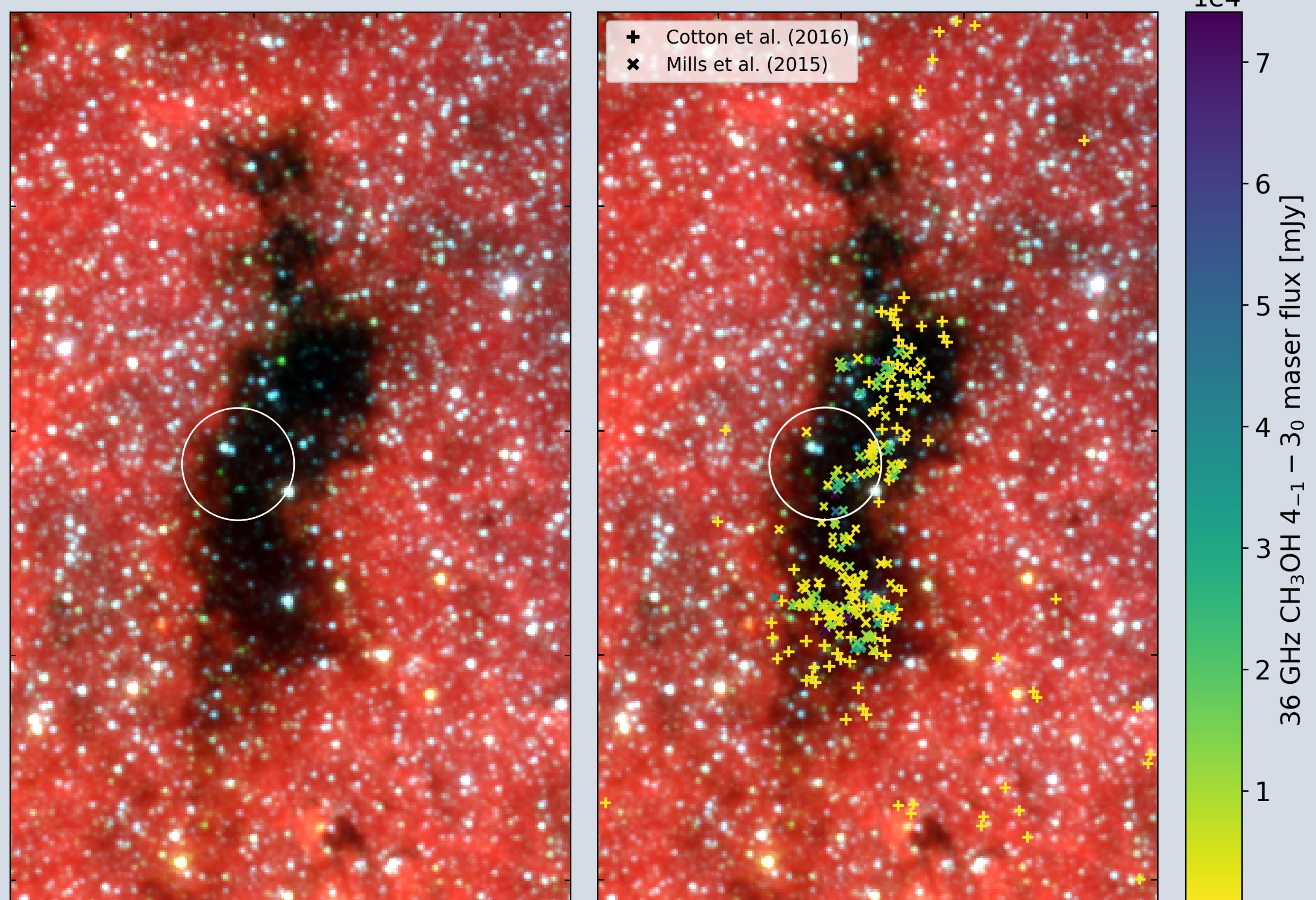


Figure 2. Left: three-color image of The Brick from Spitzer IRAC data (RGB = 8 μ m, 4.5 μ m, 3.6 μ m). The circle shows our pointing and has a radius of 30''. Right: same as left. '+'s and 'x's are locations of 36 GHz class I methanol masers from Table 2 in Cotton et al. (2016) and Table 4 in Mills et al. (2015) respectively.

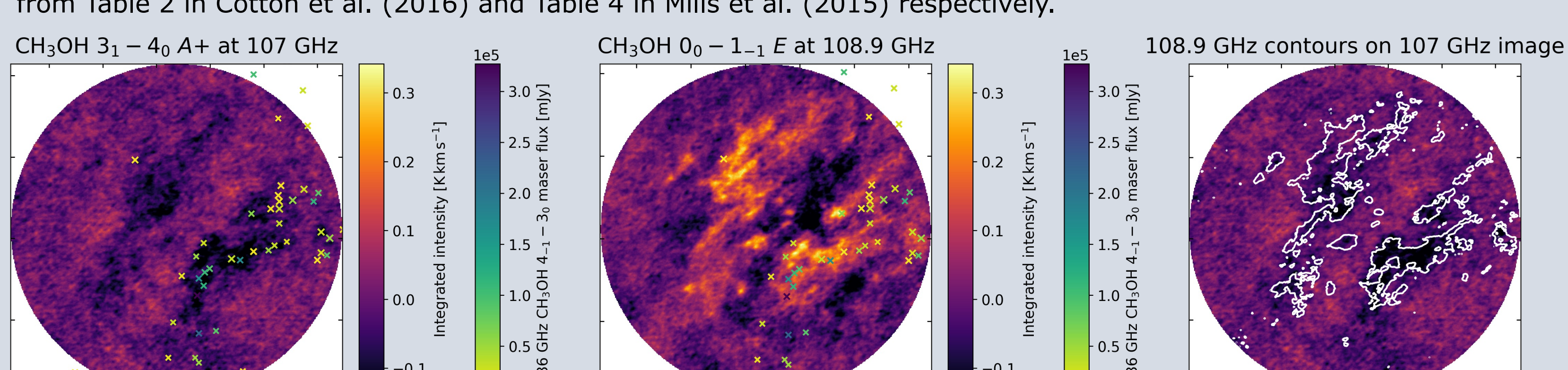


Figure 3. Comparison of 107 GHz methanol transition with nearby 108.9 GHz transition. All images are integrated intensity maps. Right panel shows the integrated intensity map of 107 GHz transition with contours of 108.9 GHz transition overlaid. Note spatial correspondence between absorption in the 107 GHz line with emission in the 108.9 GHz line. x's are 36 GHz methanol masers from Mills et al. (2015).

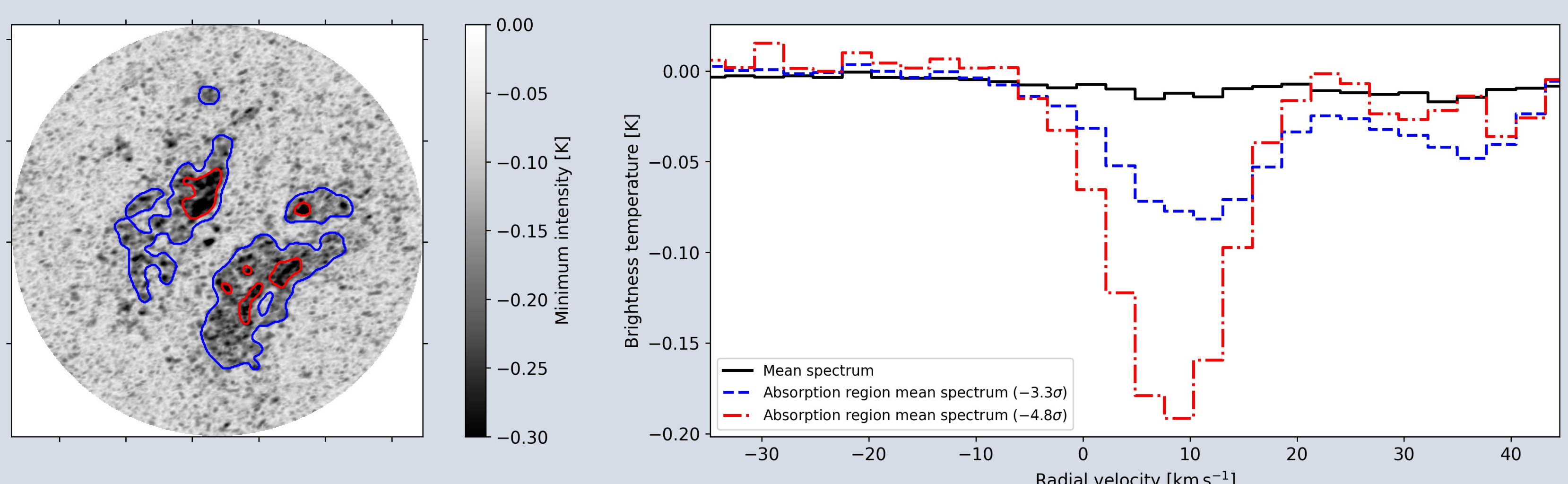


Figure 4. Spectral extraction of regions within the area where absorption is occurring. Left: minimum intensity map of 107 GHz transition. Right: spectra extracted from different regions in map: black solid line is across whole map, blue dotted line is across -3.3σ region, red dot-dashed line is across -4.8σ region.

The 107 GHz methanol transition is a dasar in The Brick

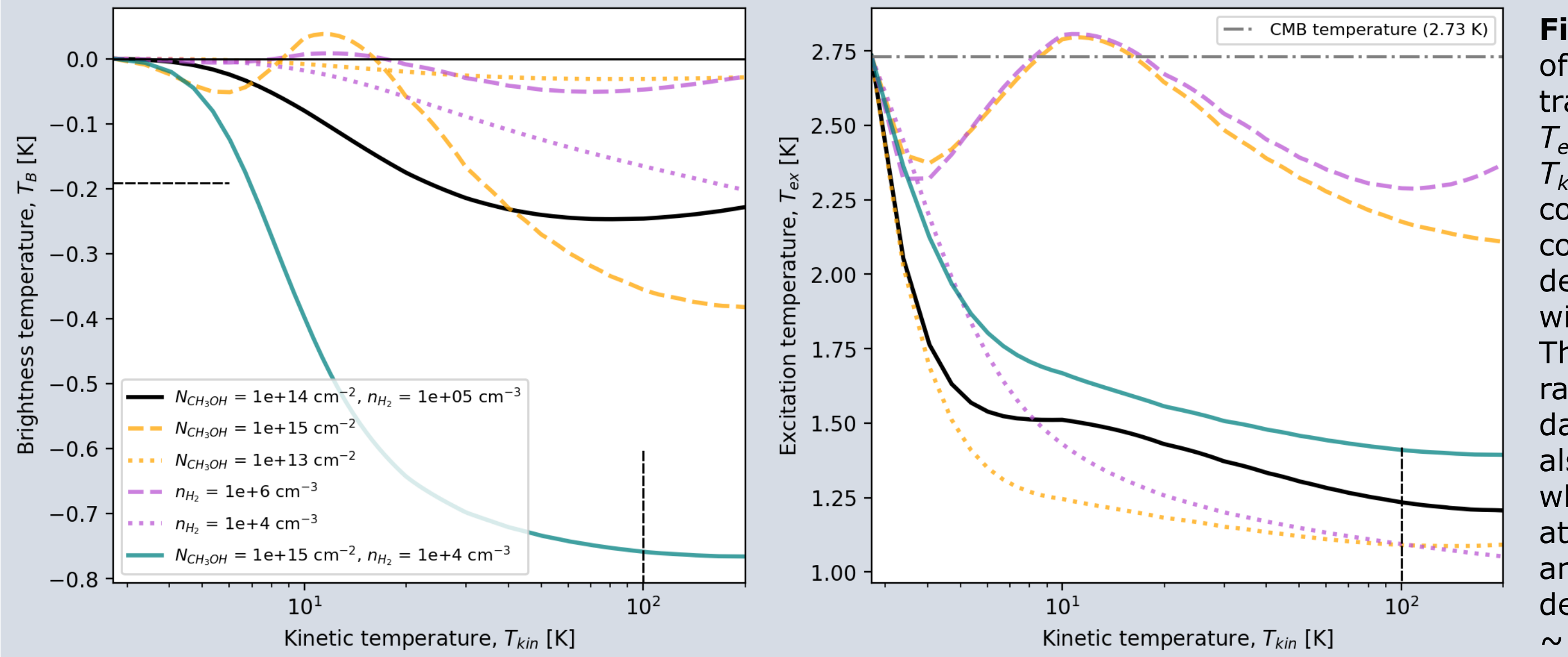


Figure 5. Behavior of the 107 GHz transition (T_B and T_{ex}) as a function of T_{kin} for several combinations of column and volume density. Modeled with pyRADEX. There are broad ranges over which dasing occurs, but also stretches where it stops (e.g., at higher column and volume densities, from $T_{kin} \sim 10$ and 20 K).

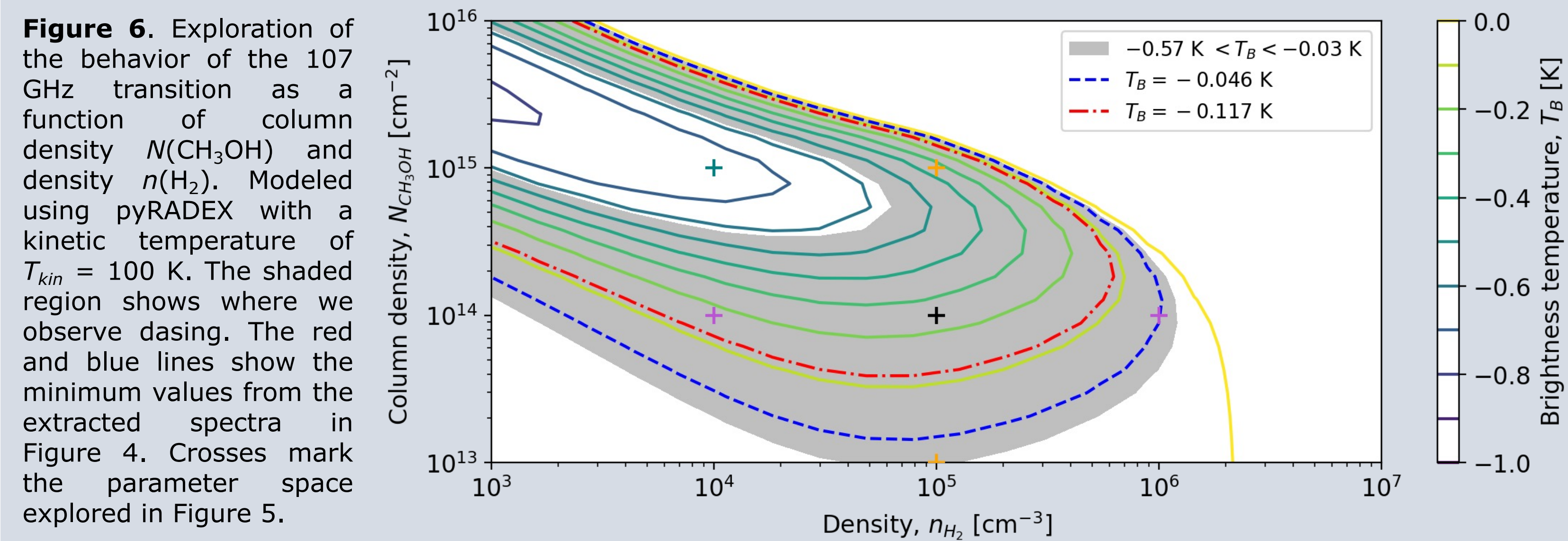


Figure 6. Exploration of the behavior of the 107 GHz transition as a function of column density $N(\text{CH}_3\text{OH})$ and density $n(\text{H}_2)$. Modeled using pyRADEX with a kinetic temperature of $T_{kin} = 100$ K. The shaded region shows where we observe dasing. The red and blue lines show the minimum values from the extracted spectra in Figure 4. Crosses mark the parameter space explored in Figure 5.

Other methanol transitions can also dase

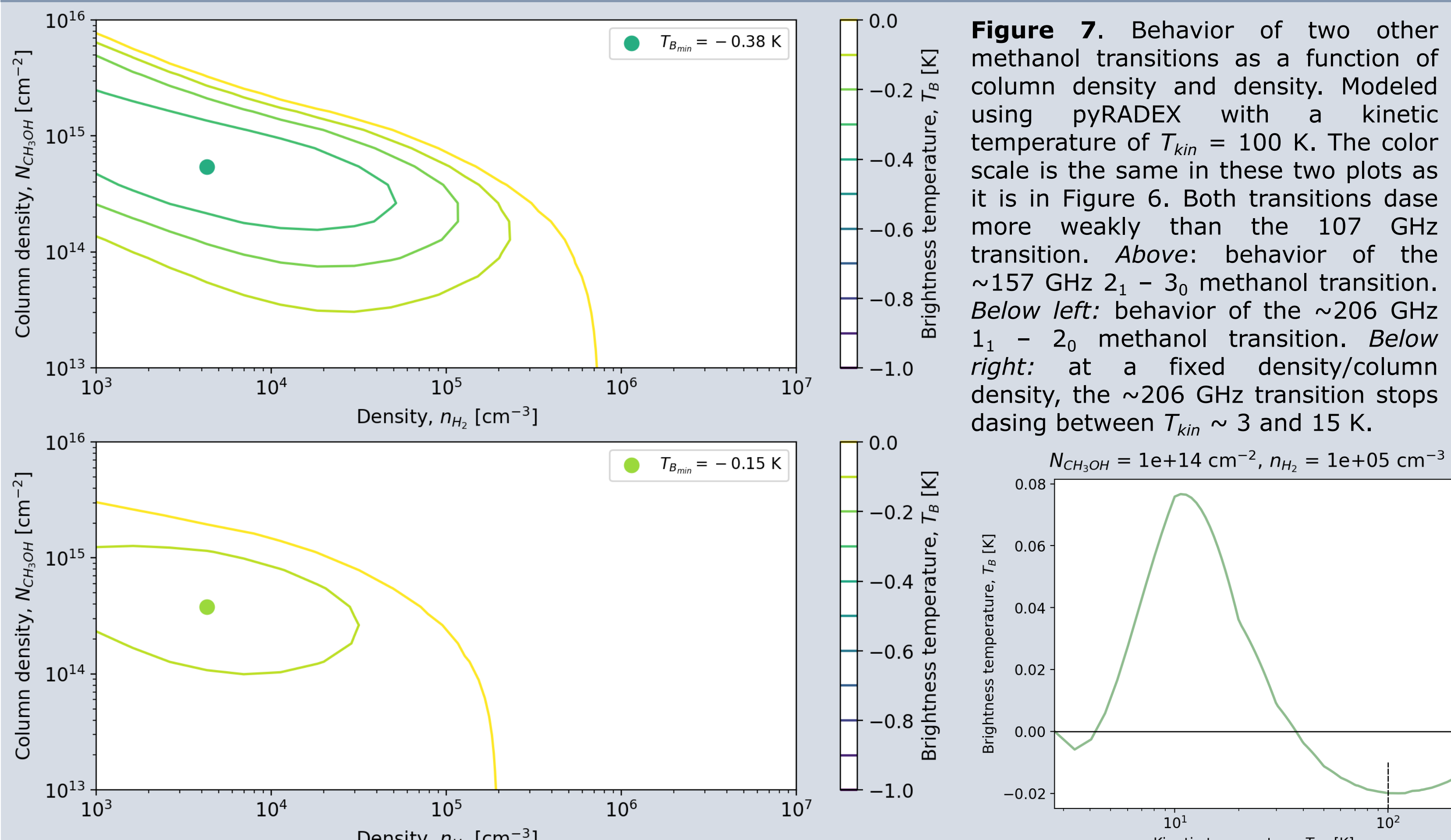


Figure 7. Behavior of two other methanol transitions as a function of column density and density. Modeled using pyRADEX with a kinetic temperature of $T_{kin} = 100$ K. The color scale is the same in these two plots as it is in Figure 6. Both transitions dase more weakly than the 107 GHz transition. Above: behavior of the ~157 GHz $2_1 - 3_0$ methanol transition. Below left: behavior of the ~206 GHz $1_1 - 2_0$ methanol transition. Below right: at a fixed density/column density, the ~206 GHz transition stops dasing between $T_{kin} \sim 3$ and 15 K.

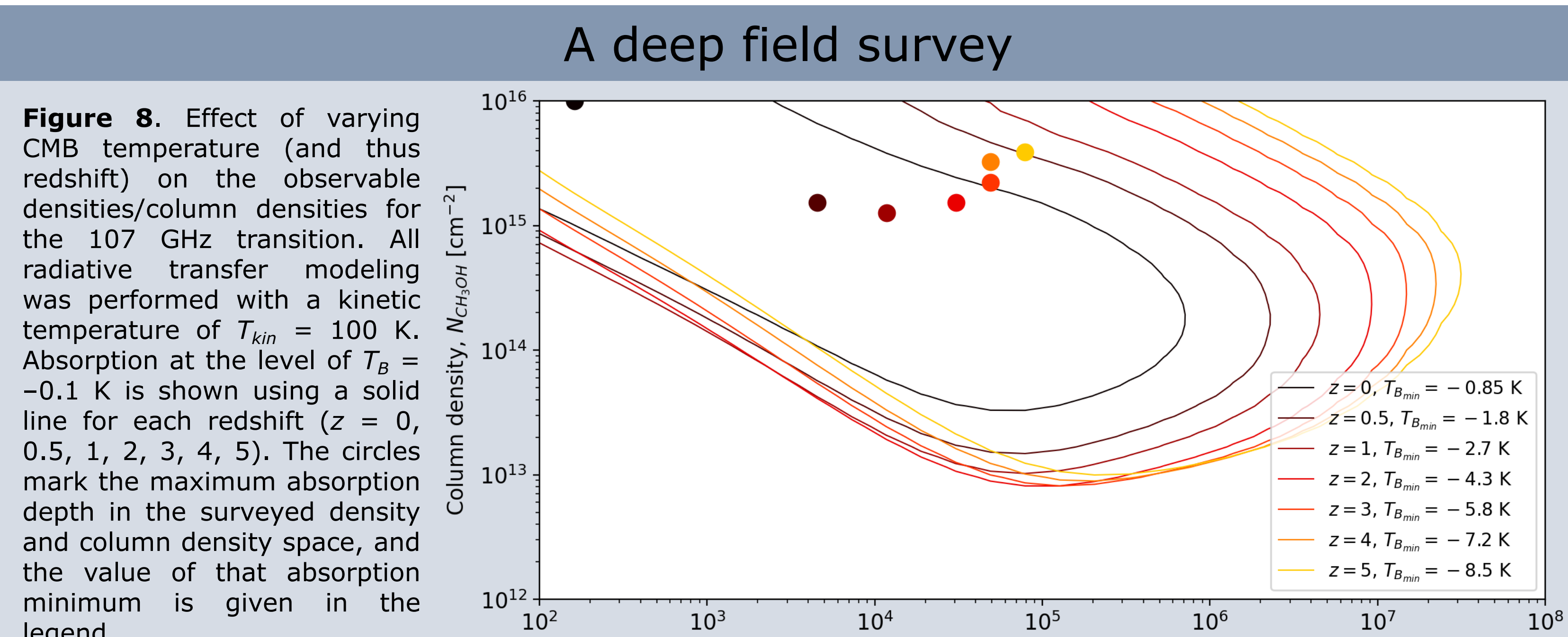


Figure 8. Effect of varying CMB temperature (and thus redshift) on the observable densities/column densities for the 107 GHz transition. All radiative transfer modeling was performed with a kinetic temperature of $T_{kin} = 100$ K. Absorption at the level of $T_B = -0.1$ K is shown using a solid line for each redshift ($z = 0, 0.5, 1, 2, 3, 4, 5$). The circles mark the maximum absorption depth in the surveyed density and column density space, and the value of that absorption minimum is given in the legend.

Configuration Targets Frequency coverage Angular resolution

ngVLA Main Interferometric Array
starbursting galaxies
~1.2 to 116 GHz
1'' (~10s of parsecs)*

*Exact angular resolution will depend on distance to target. Angular resolution should be matched to size of star-forming regions within the galaxy. Figure 2 in Darling et al. (2020) shows how various physical scales' angular size varies with redshift.

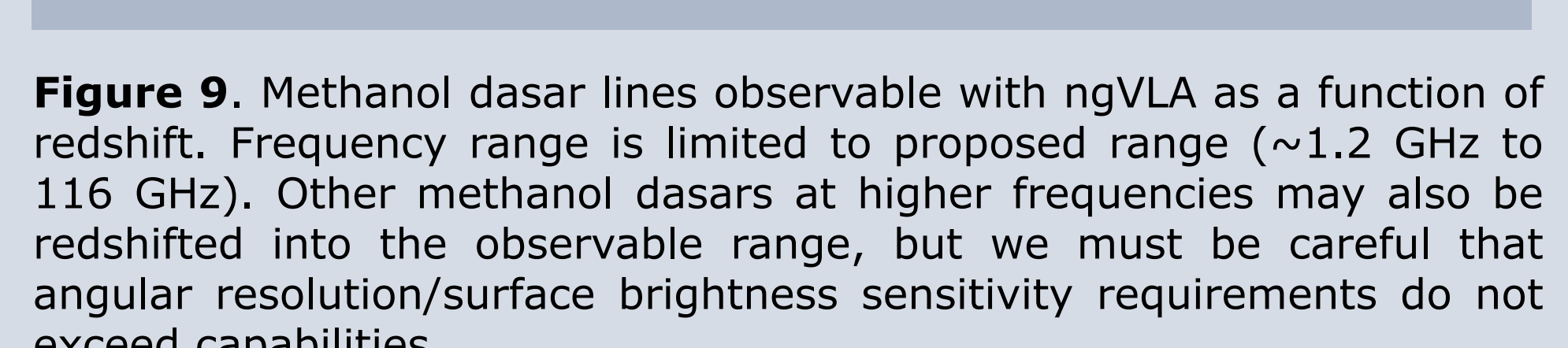


Figure 9. Methanol dasar lines observable with ngVLA as a function of redshift. Frequency range is limited to proposed range (~1.2 GHz to 116 GHz). Other methanol dasars at higher frequencies may also be redshifted into the observable range, but we must be careful that angular resolution/surface brightness sensitivity requirements do not exceed capabilities.

References

- Cotton et al. 2016, ApJS, 227, 10.
- Darling et al. 2012, ApJL, 749, L33.
- Darling 2019, Bulletin of the AAS, 51, 3.
- Ginsburg, et al. 2020, ApJS, 248, 24.
- Hunire et al. 2022, A&A, 663, A33.
- Leurini et al. 2016, A&A, 592, A31.
- Menten 1991, Astronomical Society of the Pacific Conference Series, 119–136.
- Mills et al. 2015, ApJ, 805, 72.
- Müller et al. 2005, Journal of Molecular Structure, 742, 215.
- Townes 1997, Quantum Electronics, 27, 1031.
- Turner 1991, ApJS, 76, 617.
- Val'tts et al. 1995, A&A, 294, 825.
- Walker et al. 2021, MNRAS, 503, 77.
- Walmsley et al. 1988, A&A, 197, 271.



Email: abulatek@ufl.edu

Website: abulatek.github.io